Fabrication of Rectangular Micro-Channels by Ultrashort Pulse Ablation Using a Bessel Beam

Jan Marx*[1], Jochen Tenkamp[2], Frank Walther[2], and Cemal Esen[1]

[1]*Applied Laser Technologies, Ruhr University Bochum, Universitätsstr. 150, 44801 Bochum, Germany*
[2]*Chair of Materials Test Engineering (WPT), TU Dortmund University, Baroper Str. 303, 44227 Dortmund, Germany*
**Corresponding author's e-mail: marx@lat.rub.de*

This paper reports on combining non-diffracting Bessel beams and ultra-short pulsed laser ablation for the generation of micro-channels. The small focal spot and the long focus depth make Bessel beams suitable as an ideal tool for fabricating sharp-edged channels. In this context, we present a study on the generation of rectangular micro-channels that are highly interesting for future investigations on material properties of additive manufactured and cast aluminum samples, e.g., using them as initial notches or defects, respectively, for fatigue and damage tolerance assessment. In order to achieve the highest quality of rectangular microchannels, optimal processing conditions were achieved by analyzing the influence of the laser power, the number of exposure cycles, and the axial position of the sample on the ablation process. Similar experiments using a Gaussian Beam were performed to compare the different beam shapes regarding the resulting channel geometry and ablation efficiency. Nevertheless, the walls of the Bessel beam processed channels are almost perpendicular to the surface and the bottom of the channel is almost flat. Thus, the Bessel beam generated micro-channels are more rectangular than the ones processed with the Gaussian beam.
DOI: 10.2961/jlmn.2022.03.2003
Keywords: Bessel beam, axicon, laser ablation, micro-channels, ultra-short pulse processing

1. Introduction

Due to the trend of miniaturization and the integration of functions, the fabrication of microchannels on surfaces has become more and more important in applications like microfluidic systems [1], cooling applications [2], or preparing surfaces of catalysts [3]. Depending on the application, various properties of the microchannels like surface roughness [4] and geometry [3] need to be optimized. Besides the functionalities of the micro-channels, the mechanical strength of the whole component is also affected by microchannels. This impact makes the production of microchannels on fatigue test samples highly interesting for material testing [5] due to the effect of surface roughness [6] and defects [7,8]. The precise fabrication of such predetermined breaking points helps to get insights into the effect of defects on fatigue properties, which is an upcoming research field, especially for additive manufactured and cast components [9,10].

Two things are essential for using micro-channels in material testing: First, the micro-channels need to have a clearly defined geometry with sharp corners for stress concentration. Second, the material properties should not be affected by the manufacturing approach. Therefore, a precise tool with little thermal and mechanical impact on the sample must be chosen.

In recent years, the laser has become one of the most practical tools for micro-processing surfaces [11]. Since lasers work contact-free, there is no mechanical impact on the surface, which could distort the result of the subsequent material test. However, the thermal impact of the laser beam leads to a heat-affected zone around the processed area. In order to avoid the thermal impact, ultrashort pulse (USP) lasers are used to ablate material by so-called cold ablation. Thus, the material around the channel remains unchanged in its mechanical and chemical properties and the melt expulsion is reduced to a minimum [12].

For precisely processing the rectangular shape of the microchannels, a suitable beam shaping method must be chosen. The most frequently used beam shaping method for ablation processes is focussing a Gaussian-shaped beam by a convex lens or a combination of spherical lenses, respectively [1,13,14]. Although Gaussian beam applications have convinced by an easy alignment and cheap optical components compared to other beam shapes, their suitability for the fabrication of rectangular microchannels is limited due to diffraction effects. A rectangular shape is difficult to achieve with Gaussian beams because the spatial intensity distribution across the Gaussian beam affects the shape of the ablation crater when processing material. It is not preferable to focus a Gaussian beam to smaller spots, since it reduces the focal length, which needs to be high for high aspect ratio microchannel fabrication.

Bessel beams can be used instead of Gaussian beams to overcome the above-mentioned difficulties. Bessel beams are a diffraction-free solution of the Helmholtz equation [15]. Although ideal Bessel beams cannot be generated experimentally, Bessel-Gauss beams can be generated by sending a Gaussian beam through an axicon lens [16] for processing below the diffraction limit [17]. Further, a 4f telescope objective can be added to an axicon-based optical

setup in order to demagnify the spot size of the central core of a Bessel beam to the range of 2 µm and below [18,19]. At the same time, the propagation length can reach several millimeters. These properties make the Bessel beam an exciting tool for applications with deep penetration of the material, e.g., glass dicing [20] or micro-drilling [21,22]. For the latter, the generation of steep walls and high aspect ratio ablation has been proven many times [22,23].

However, few works concerning the fabrication of microchannels using a Bessel beam have been published. Kumar et al. used Bessel beams to generate microstructures on synthetic diamond samples [24]. In this case, a single pass track was sufficient for their experiments to create a deep channel. The deep ablation effect is well known in the process of transparent material [19,25,26]. Contrary, for non-transparent media, the ablation depth is lower, and even the total depth of Bessel beam ablation processes is limited since shielding effects prevent part of the conical wavefront from propagating into deep structures [27]. Nevertheless, Alexeev et al. showed by simulation, that there is still deep propagation inside narrow holes due to reflections at the side walls of the hole [21].

This work presents a Bessel beam-based method for producing high aspect ratio microchannels having a rectangular shape on aluminum. A multi-path writing strategy was used for the experiments. In the first step, the fabrication of microchannels using Bessel beams on additively manufactured aluminum samples was demonstrated. A further parameter study on cold-rolled aluminum samples showed scope for adjusting the depth of the generated channels. Finally, comparing experiments with Gaussian beams were performed to identify the strength and weaknesses of both microchannel fabrication techniques.

2. Methods

The additively manufactured AlSi10Mg aluminum samples were processed vertically by laser-beam powder bed fusion (PBF-LB) at a Trumpf system TruPrint 1000 at the Fraunhofer Research Institution for Additive Manufacturing Technologies (IAPT, Germany, Hamburg).

Afterwards, the aluminum samples were processed using an 800 nm Ti:Sa-Laser (Spitfire Ace, Spectra-Physics). The laser emits pulses with a minimum width of 100 fs. The internal pulse stretcher of the laser allowed to reduce the temporal broadening of the pulse due to dispersion. The beam shaping setup is illustrated in Fig. 1. The Gaussian output beam of the laser (diameter 8.3 mm at $1/e^2$, M^2 = 1.11) was transformed into a Bessel beam using an axicon with a base angle α of 5° (Thorlabs AX255-B). In order to increase the intensity of the Bessel beam, a telescope objective consisting of two convex lenses (f_1 = 160 mm, f_2 = 20 mm) was integrated in the far-field behind the axicon. The distance between the axicon tip and the first lens of the telescope is the sum of the half length of the Bessel zone (z_{max} = 104.4 mm) plus the the focal length of the lens. Thus, the secondary Bessel beam behind the last lens was demagnified by a factor of 8 compared to the Bessel beam initially generated by the axicon. The calculated resulting central core diameter of the processing Bessel beam was 1.4 µm ($1/e^2$) and the length z_{max2} of the Bessel zone was 1.6 mm. Nitrogen was used as a process gas with lateral feed. The gas flew out of a tube (diameter 6.5 mm) with a pressure of 1.5 bar. The tube was placed right beside the processing area.

The samples were placed on an xyz-stage (M-521.DD for the x-axis and z-axis, M-511.DG for the y-axis, all from Physik Instrumente (PI)). The relative movements between the laser beam and the sample were realized by moving the stage. Although a Galvano scanner could be used instead of a mechanical stage in order to reach faster relative movements between the beam and the sample [28], it was not used for two reasons: First, the repetition rate of the laser was 5,000 Hz, which limited the speed of the process. Thus faster movements were not required. Second, the number of optics was reduced to a minimum in order to avoid affecting the temporal and spatial pulse shape by any further optical component.

The z-axis of the stage was set parallel to the optical axis (see fig. 1). Thus, it allowed adjusting the distance of the sample surface to the objective lens. This distance was set once for each experiment and remained unchanged during the process. During the experiments, the sample was moved in the xy-plane with a constant speed of 0.1 mm/s. One exposure cycle consists of 30 lines parallel to the microchannels direction. The hatch distance between the lines was 1.33 µm. Thus, the total stage movement in the x-direction was 40 µm. The stage was moved alternating from left to right and right to left with a half hatch distance offset.

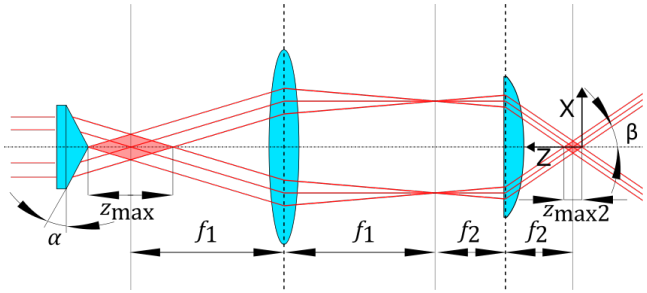

Fig. 1 Schematic beam shaping setup containing an axicon (α = 5°) and two convex lenses (f_1 = 160 mm, f_2 = 20 mm), the effective cone angle β of the Bessel beam is 17.7°.

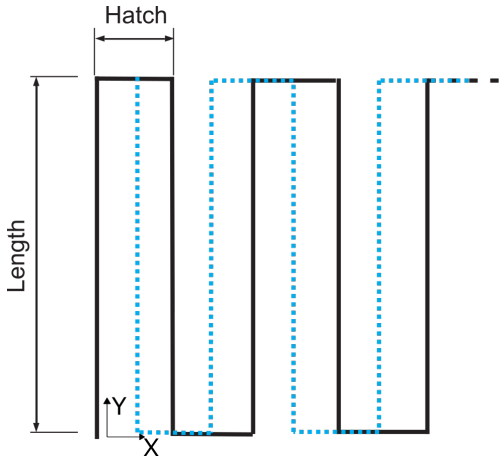

Fig. 2 Schematic writing path for the ablation. The black line shows the first exposure cycle runs from left to right. The dashed blue line shows the second cycle runs opposite.

With the mentioned parameters, the lines of two consecutive exposure layers had an overlap area of 48 % of the spot size. The way of fabricating two exposure layers is demonstrated in fig. 2. The length of the channels was set to 1 mm for the first experiments. 20 exposure cycles were used.

After the process was finished, the samples were put into an ultrasonic cleaning bath to remove particles from the microchannels. Afterward, the shape of the structures generated was analyzed using a laser-scanning microscope (Olympus LEXT OLS 5000). Finally, detailed images of the sample surface were taken using a scanning electron microscope (Zeiss EVO MA10).

3. Results and discussion

An SEM image of a micro-channel processed with the parameters mentioned in section 2 is shown in fig. 3a. It can be seen that the width of the channel is slightly larger than the moving path of the stage. Thus, higher-order maxima of the Bessel beam seem to contribute to the ablation process. Fig. 3c shows the topography of the generated structure. A sectional view is presented in fig. 3b. At the edge of the channel, where the moving path of the stage changed the direction, unevenness occurred at the bottom of the channel. The unevenness was due to the acceleration of the stage axis. The acceleration effects could be avoided by skywriting [29], but this was technically not possible for the setup used. Thus, only the middle two-thirds of the channel were considered for measurement of the channel depth. The measurement of the channel depth was done using a 3D laser-scanning microscope. The channel depth was averaged to a level of compensation (black frame in fig. 3c) and the vertical distance to the untreated surface was calculated. For the given sample, the depth of the microchannel was 165 µm. The slightly asymmetric shape of the channel bottom was caused by the direction of the process gas flow. This assumption was proofed by changing the gas flow direction to the opposite, which lead to a mirrored resulting channel shape.

For optimizing the aspect ratio of the generated microchannels, the axial position of the sample surface, the average laser power, and the number of exposure cycles were varied. Changing the hatch distance or the number of parallel lines in one exposure cycle to smaller values was no option since the channel needs a specific width to avoid a shielding effect that prevents the beam from propagating inside the channel. Cold-rolled aluminum samples were used for the experiments in sections 3.1 to 3.4. The length of the micro-channels was reduced to 300 µm.

3.1 Variation of the focal position

In this section, the axial position of the sample was varied. The ring beam refracted by the last lens has a diameter close to the diameter of the lens. Due to the spherical form of the lens, the ring beam was refracted to a shorter focus than the nominal focal length of 20 mm. However, spherical aberration was not a problem since there was no intensity in the center of the lens and the width of the ring beam was quite narrow. The nominal focus point 20 mm behind the lens was defined as the coordinate origin for this study.

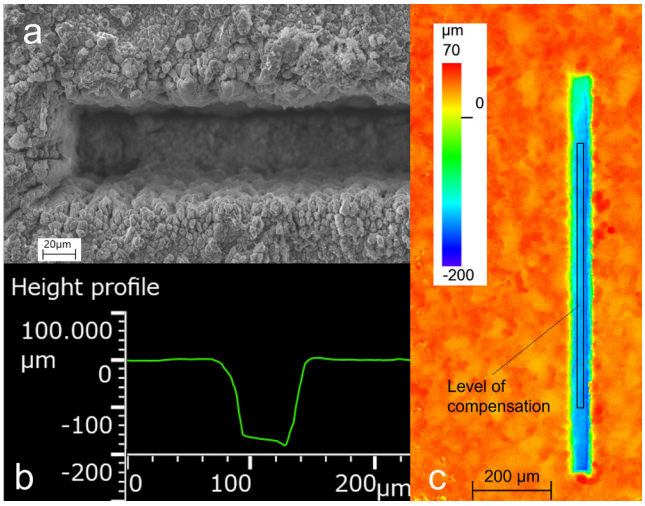

Fig. 3: a) SEM image of a micro-channel on an additively manufactured AlSi10Mg sample; b) Cross-section of the microchannel measured with a 3D laser-scanning microscope; c) topography map measured with a 3D laser-scanning microscope

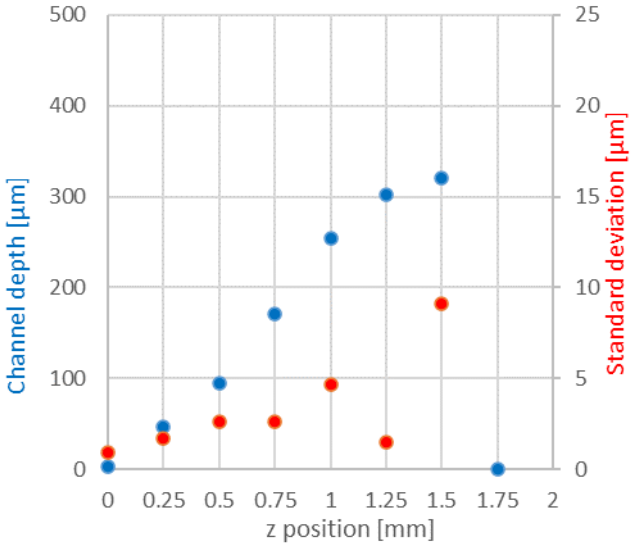

Fig. 4 Channel depth and standard deviation for different axial positions of the sample

The average power was set to 3 W and the number of exposure cycles was set to 10. The axial sample position was varied in steps of 0.25 mm in a range between 0 mm and 1.75 mm. The mean value of measured channel depths was calculated using three samples. The results are illustrated in the diagram in fig. 4.

The diagram shows increasing channel depth for samples placed closer to the lens. The standard deviation for all z-positions up to 1.25 mm was below 5 µm. The deepest channels could be generated at 1.5 mm. The average depth at this point was 321 µm. However, the standard deviation of 9.1 µm at this point was significantly higher. A possible explanation for the increase in standard deviation can be given by the work of Wu et al. [30]. They investigated that the non-perfect tip of physical axicons leads to axial intensity oscillations when setting the working distance closer to the axicon. Above 1.5 mm, the channel depth was close to

zero, since the sample surface was placed out of the Bessel zone. Thus, the intensity was too low to ablate the material.

The position of 1.25 mm was used for further experiments. Again, it was because of the high channel depth combined with a small standard deviation.

3.2 Variation of Laser power

The next parameter varied was the laser power. It was raised from 0.5 W average power to 4.0 W in steps of 0.5 W. Again, three samples were processed with each parameter and the channels were analyzed. Fig. 5 shows the resulting channel depth for the different laser powers.
As expected, the depth of the microchannels increased at higher laser power. The correlation was approximately linear. However, the standard deviation increased at high laser powers, too. The high standard deviation can be explained by increasing heat input causing melt splashes for samples processed with more than 3 W. This effect can be associated with the influence of the higher-order maxima rings of the Bessel beam, which do not ablate much material, but carry enough energy to heat up the process zone. Thus, the average laser power was set to 3 W for further experiments to have a good compromise between high ablation depth and good surface quality.

3.3 Variation of exposure cycles

In order to increase the energy input without using higher average laser power, the number of exposure cycles was varied instead. The experiments were carried out three times using 3 W average laser power and an axial sample position of 1.25 mm. The channel depth and its standard deviation are plotted in fig. 6. The graph in fig. 6 shows a monotonously increasing, but degressive trend. The curve has a logarithmic course in good approximation. Thus, the total ablation efficiency decreases with greater channel depth. Two exposure cycles lead to an ablation depth of

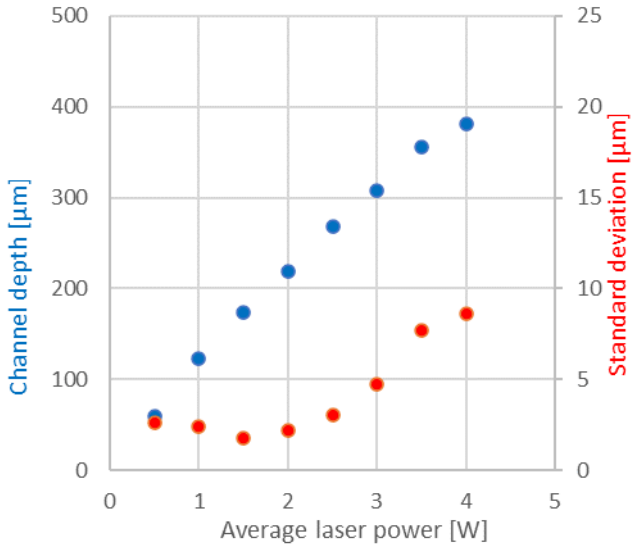

Fig. 5 Channel depth and standard deviation for different average laser power.

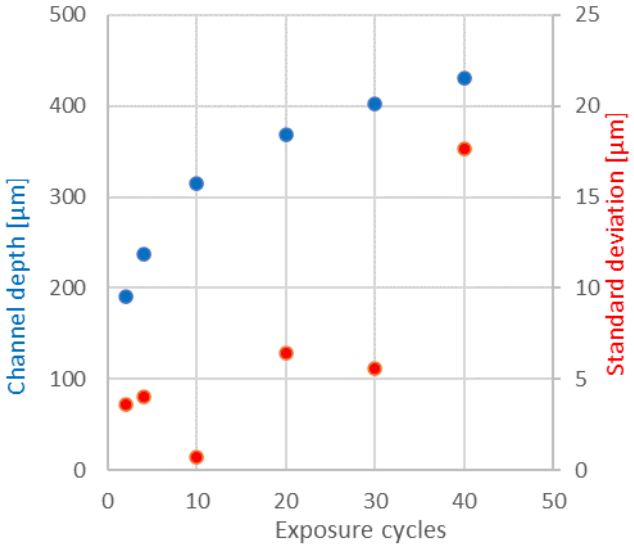

Fig. 6 Channel depth and standard deviation for different numbers of exposure cycles

190 µm, which was more than half of the total ablation depth of the experiment with 20 exposure cycles. Possible reasons for the degressive trend of the curve are shielding effects [27] and the problem of ablated material redeposited in deeper channels. The latter could also explain the huge standard deviation for the experiments with 40 exposure cycles.

3.4 Comparison with Gaussian beam

In order to evaluate the quality of the Bessel beam processed microchannels, similar experiments were carried out with a Gaussian beam. Therefore, a strategy allowing a comparison of the different beam shapes had to be found. Usually, the peak fluence is the relevant parameter for comparing different ablation processes. Because the given work deals not with ablation at the surface, but with deep channels, there are some problems for comparing peak fluences. First, it is not possible to get the same peak fluence for both beam shapes during the whole process of microchannel generation, since the depth of focus is much smaller for the Gaussian beam compared to the Bessel beam. Thus, the Bessel beam keeps its high focal intensity when the channel gets deeper during the process. The Gaussian beam, however, has its highest intensity at the focus and is diverging behind it. Therefore, defining processes with similar peak fluences or peak intensities is not reasonable.

Second, the intensity distribution inside high aspect ratio structures does not follow the rules of geometric optics. Diffraction and multiple and diffuse reflections at the channels walls make the intensity distribution become more homogenous inside the microchannels [31,32]. Thus, processes with equal average laser power inside the channel were chosen for comparison.

The Bessel beam processed channels from section 3.2 with 500 mW average laser power were used for the comparison. A single convex lens with a focal length of 30 mm was used for the Gaussian beam experiments. The focal spot size is approximately 4 µm ($1/e^2$) for the given setup. Due to the small focus, the focus depth is only 14 µm.

Beam path, material, and all laser parameters except the average laser power were the same for both beam shapes. The Bessel beam carries only approximately 30 % of its energy in the central core. The higher-order maximum rings carry the rest of the energy. In order to have the same energy carried in the central core for the Bessel beam and the Gaussian beam experiments, the average laser power for the Gaussian beam experiments was reduced to 150 mW.

The topography of both microchannels was measured with a laser scanning microscope. Fig. 7 shows the cross-section of both channels in comparison. Although the laser power was reduced for the Gaussian beam experiments, the micro-channel was deeper. The width of both channels was almost the same. However, the geometry of the Bessel beam processed micro-channels was much more rectangular. The Gaussian processed microchannel had an almost conical shape, especially at the bottom of the channel. The Bessel beam processed microchannel had an almost flat plateau at the bottom of the micro-channel. The variation in depth was only approximately 5 µm over a width of 35 µm.

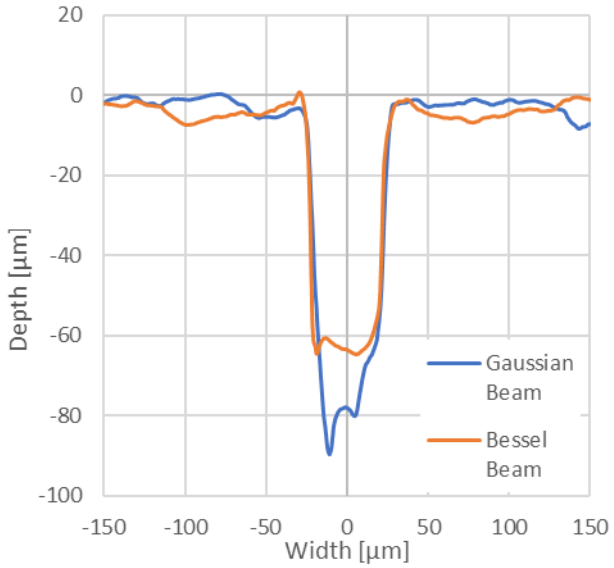

Fig. 7 Cross-section of micro-channels processed with Gaussian beam and Bessel beam

4. Conclusion

A process for the generation of micro-channels on metal surfaces using a Bessel beam was successfully demonstrated. The channel depth could be adjusted up to 400 µm by changing the laser power, axial sample position, or the number of exposure cycles. All three parameters investigated are subject to limits in terms of the achievable channel depth. In this context, process instabilities resulting in higher standard deviations of the total channel depth and worse surface quality can be named as possible reasons for such limitations.

Although the ablation efficiency of the Bessel beam generated microchannels is reduced due to the unused energy carried by the higher order maxima, the rectangularity of the channels could be improved significantly by using a Bessel beam. While the Gaussian beam process inevitably leads to a conical-shaped channel cross-section, the Bessel beam processed micro-channel has an almost flat plateau at the bottom. Thus, they are an ideal tool for notching specimens for material tests.

Acknowledgments

We gratefully acknowledge funding by the German Federal Ministry for Economic Affairs and Climate Action (BMWK) under grant 16KN053050 and the German Research Founation (DFG) under grants 282318703 and 425479688. Further thanks to the Fraunhofer Research Institution for Additive Manufacturing Technologies (IAPT) for the supply of sample manufacturing within an excellent scientific collaboration.

References

[1] D. Lim, Y. Kamotani, B. Cho, J. Mazumder, and S. Takayama: Lab Chip, 3, (2003) 318.
[2] W. Yu, M. Desmulliez, A. Drufke, M. Leonard, R. Dhariwal, D. Flynn, G. Bognar, A. Poppe, G. Horvath, Z. Kohari, and M. Rencz: J. Micromech. Microeng., 20, (2009) 025004.
[3] Y. Ke, W. Zhou, X. Chu, D Yuan, S. Wan, W. Yu, and Y. Liu: Int. J. Hydrog. Energy, 44, (2019) 5755.
[4] D. Teixidor, I. Ferrer, J. Ciurana, and T. Özel: Robot. Comput. Integr. Manuf., 29, (2013) 209.
[5] X. Zhu, J. Jones, and J. Allison: Metall. Mater. Trans. A, 39, (2008) 2666.
[6] D. Kotzem, P. Dumke, P. Sepehri, J. Tenkamp, and F. Walther: Prog. Addit. Manuf., 5, (2020) 267.
[7] D. Kotzem, S. Kleszczynski, F. Stern, A. Elspaß, J. Tenkamp, G. Witt, and F. Walther: Int. J. Fatigue, 148, (2021) 1.
[8] J. Tenkamp, F. Stern, and F. Walther: Addit. Manuf. Lett., 3, (2022) 100054.
[9] E. Wycisk, A. Solbach, S. Siddique, D. Herzog, F. Walther, and C. Emmelmann: Phys. Procedia, 56, (2014) 371.
[10] K. Solberg and F. Berto: Int. J. Fatigue, 137, (2020) 105637.
[11] S. Prakash and S. Kumar: Proc. Inst. Mech. Eng. B J. Eng. Manuf., 229, (2015) 1273.
[12] K. Leitz, B. Redlingshöfer, Y. Reg, A. Otto, and M. Schmidt: Phys. Procedia, 12, (2011) 230.
[13] P. Zhang, L. Chen, J. Chen, and Y. Tu: Opt. Lasers Eng., 98, (2017) 69.
[14] M. Pfeifenberger, M. Mangang, S. Wurster, J. Reiser, A. Hohenwarter, W. Pfleging, D. Kiener, and R. Pippan: Mater. Des., 121, (2017) 109.
[15] J. Durnin, J. Miceli, and J. Eberly: Phys. Rev. Lett., 58, (1987) 1499.
[16] G. Indebetouw: J. Opt. Soc. Am. A, 6, (1989) 150.
[17] B. Yalizay, T. Ersoy, B. Soylu, and S. Akturk: Appl. Phys. Lett., 100, (2012) 031104.
[18] A. Marcinkevičius, S. Juodkazis, S. Matsuo, V. Mizeikis, and H. Misawa: Jpn. J. Appl. Phys., 40, (2001) L1197.
[19] T. Chen, G. Zhang, Y. Wang, X. Li, R. Stoian, and G. Cheng: Micromachines, 11, (2020) 671.
[20] J. Dudutis, J. Pipiras, S. Schwarz, S. Rung, R. Hellmann, G. Račiukaitis, and P. Gečys: Opt. Express, 28, (2020) 5715.

[21] I. Alexeev, K.-H. Leitz, A. Otto, and M. Schmidt: Phys. Procedia, 5, (2010) 533.
[22] H. Nguyen, E. Moreno, A. Rudenko, N. Faure, X. Sedao, C. Mauclair, J. Colombier, and R. Stoian: Sci. Rep., 12, (2022) 1.
[23] M. Kohno and Y. Matsuoka: JSME Int. J. B., 47, (2004) 497.
[24] S. Kumar, S. Eaton, M. Bollani, B. Sotillo, A. Chiappini, M. Ferrari, R. Ramponi, P. Di Trapani, and O. Jedrkiewicz: Sci. Rep., 8, (2018) 1.
[25] H. Wang, F. Zhang, and K. Ding: Optik, 229, (2021) 166295.
[26] Q. Xie, X. Li, L. Jiang, B. Xia, X. Yan, W. Zhao, and Y. Lu: Appl. Phys. A, 122, (2016) 1.
[27] Y. Matsuoka, Y. Kizuka, and T. Inoue: Appl. Phys. A, 84, (2006) 423.
[28] H. Nguyen, X. Sedao, C. Mauclair, G. Bidron, N. Faure, E. Moreno, J. Colombier, and R. Stoian: Micromachines, 11, (2020) 974.
[29] R. De Loor: Phys. Procedia, 41, (2013) 544.
[30] P. Wu, C. Sui, and W. Huang: Photonics Res., 2, (2014) 82.
[31] Y. Qin, A. Michalowski, R. Weber, S. Yang, T. Graf, and X. Ni: Opt. Express, 20, (2012) 26606.
[32] D. Förster, R. Weber, D. Holder, and T. Graf: Opt. Express, 26, (2018) 11546.

(Received: May 31, 2022, Accepted: October 31, 2022)